

Electromagnetic fluxes, monopoles, and the order of the $4d$ compact $U(1)$ phase transition.

Michele Vettorazzo^{a,1} and Philippe de Forcrand^{a,b,2}

^a*Institute for Theoretical Physics, ETH Zürich, CH-8093 Zürich, Switzerland*

^b*CERN, Theory Division, CH-1211 Genève 23, Switzerland*

Abstract

We consider the $4d$ compact $U(1)$ gauge theory with extended action

$$S = -\beta \sum_P \cos \theta_P - \gamma \sum_P \cos 2\theta_P$$

We give a full characterization of the phase diagram of this model using the notion of *flux*. The relation with the usual monopole picture is discussed. In analogy with the XY model we consider the *helicity modulus* [1] for this theory, and show that it is an order parameter. Analyzing the finite-size effects of the helicity modulus we conclude that the transition is first-order. The value of this order parameter is related to the renormalized coupling β_R . We measure β_R^c at the transition point and give a counterexample to its conjectured universal value [2].

¹vettoraz@phys.ethz.ch

²forcrand@phys.ethz.ch

1 Introduction

A phase transition in an infinite system is rigorously defined by a non-analyticity of the free energy as a function of the driving parameter (like the temperature, an external field or some coupling of the theory). In practice, a useful description can be provided by identifying an observable (the so-called *order parameter*) whose vacuum expectation value is zero in one phase and non-zero in the other. This behavior is manifestly non-analytic and can sometimes be used to relate the phase transition with the spontaneous breaking of some symmetry (implicitly or explicitly defined) of the model, thus providing an appealing physical picture of the transition itself.

The formulation of an order parameter is a highly non-trivial problem, and closely depends on the specific features of the theory considered. A broad class of theories (for a review see [3]), which includes the $4d$ compact Abelian theory we are going to consider, admits a characterization of the transition in terms of *topological defects*, which is a general name used to indicate some collective degrees of freedom with non-trivial homotopy group in terms of which one tries to reformulate the partition function of the system: the picture which emerges is a theory of interacting defects (sometimes one says that there is a *gas of defects*), which are very dilute in one phase and are condensed in the other. The nature of such a description is truly non-perturbative.

An open question is the following: is the choice of the excitation responsible for the phase transition unique? or is there some freedom in the identification of the topological structure involved? Here, we consider this question for the compact $U(1)$ system on a hypertorus.

In $3d$, a convenient choice of defect is the pointlike *magnetic monopole* [4]; in $4d$ we naturally have, instead of pointlike objects, *monopole currents* representing monopoles evolving in space-time. The partition function of the theory can be expressed in terms of these currents [5] and the following picture emerges: in addition to a weak-coupling Coulomb phase in which only small and dilute loops are present, one finds a strong-coupling confined phase in which there are many monopole loops deeply entangled.

Suppose now that one monitors the value of the electromagnetic (e.m.) *flux* through some plane; we expect to observe two completely different situations in the two regimes: the flux should be constant if no monopoles are present, while it should dramatically vary in the other phase. This is the physical picture we are going to consider, namely a picture of the phase transition in terms of fluxes and not in terms of monopoles: they are equivalent from the logical point of view; there can then be arguments in favor of one or the other picture, but none ‘precedes’ the other in a strict logical sense.

As we will extensively see, this alternative point of view provides a way to define a natural order parameter for the system, the so-called *helicity modulus*, defined by

the response of the system to a variation of the flux. An accurate determination of this observable will be used as the basis for a finite-size effect analysis, which will provide good evidence about the first-order nature of the transition.

The paper is organized in the following way. In sections 2 and 3 we review the model under study and the notion of flux on a lattice. In section 4 we show how the behavior of fluxes qualitatively changes across the phase boundaries of the system, and thus provide a first characterization of the model in terms of fluxes. We also interpret this behavior in terms of the monopole picture, showing the equivalence of the two approaches (we will not review the monopole picture [4] [5], but only use some results to interpret our data). In section 5 we develop an analogy between our Abelian context and the non-Abelian one, proposing the analog of 't Hooft's twisted boundary conditions [6]. In section 6 we introduce an order parameter for our theory, the helicity modulus [7]. In section 7 we show our numerical results for the order parameter in the whole phase diagram; in the following three sub-sections we discuss (i) the issue of the order of the phase transition, (ii) the relation between the helicity modulus and the renormalized coupling (in the Coulomb phase), and (iii) the conjecture (first proposed by Cardy [2]) about the universality of its value at the transition. In section 8 we show how the presence of a monopole in the lattice can be enforced by adding a flux and using C-periodic boundary conditions; the free energy of a monopole is studied and a comparison with other constructions is presented. Conclusions follow. Preliminary results about sections 2-5 have been presented in [8]. In Table 3 in the Appendix we present a summary of the simulations performed for the paper.

2 The model

Consider a $4d$ lattice with periodic boundary conditions (p.b.c.). Call a the lattice spacing. We associate to links a $U(1)$ field $U_\mu(r) = \exp(i\theta_\mu(r)) = \exp(iaeA_\mu(r))$, where e is the gauge coupling, $r = ax_\mu\hat{e}_\mu$ ($x_\mu = 1, \dots, L_\mu$) and \hat{e}_μ is the unit vector in direction $\mu = 1, \dots, 4$. We work with the following action:

$$S = -\beta \sum_P \cos \theta_P - \gamma \sum_P \cos 2\theta_P \quad (1)$$

where $\theta_P \equiv \theta_{\mu\nu}(r) = \theta_\mu(r) + \theta_\nu(r + \hat{e}_\mu) - \theta_\mu(r + \hat{e}_\nu) - \theta_\nu(r)$ is the plaquette angle, β is the Wilson coupling, and we refer to γ as the *extended* coupling. This model was introduced by Bhanot [9] and has attracted interest also recently [10].

In order to point out the symmetries of the model consider the following transformation of link variables

$$\begin{aligned}
U_1(x, y, z, t) &\rightarrow U_1(x, y, z, t) \\
U_2(x, y, z, t) &\rightarrow \begin{cases} \tilde{U} \cdot U_2(x, y, z, t) & \text{if } x \text{ is odd} \\ U_2(x, y, z, t) & \text{if } x \text{ is even} \end{cases} \\
U_3(x, y, z, t) &\rightarrow \begin{cases} \tilde{U} \cdot U_3(x, y, z, t) & \text{if } x + y \text{ is odd} \\ U_3(x, y, z, t) & \text{if } x + y \text{ is even} \end{cases} \\
U_4(x, y, z, t) &\rightarrow \begin{cases} \tilde{U} \cdot U_4(x, y, z, t) & \text{if } x + y + z \text{ is odd} \\ U_4(x, y, z, t) & \text{if } x + y + z \text{ is even} \end{cases} \quad (2)
\end{aligned}$$

where \tilde{U} is a $U(1)$ matrix at will. This transformation is such that

- if $\tilde{U} = -1 = e^{i\pi}$ every configuration with couplings (β, γ) is mapped into one with couplings $(-\beta, \gamma)$. But since this is just a change of variables, we conclude that the mapping $\beta \rightarrow -\beta$ is a symmetry of the theory.
- if $\tilde{U} = e^{i\frac{\pi}{2}}$ we map $(0, \gamma) \rightarrow (0, -\gamma)$, which is therefore another symmetry.

Furthermore, the change of variables $\theta_\mu(x) \rightarrow 2\theta_\mu(x)$ maps the couplings $(\beta, 0)$ onto $(0, \beta)$, showing the equivalence of the model on the two coordinate axes.

Finally, the limit $\gamma \rightarrow +\infty$ corresponds to recovering the Z_2 gauge theory ($\theta_P = \{0, \pi\}$); a gauge-transformation then fixes the links to Z_2).

In Fig. 1 we draw a sketch of the phase diagram.

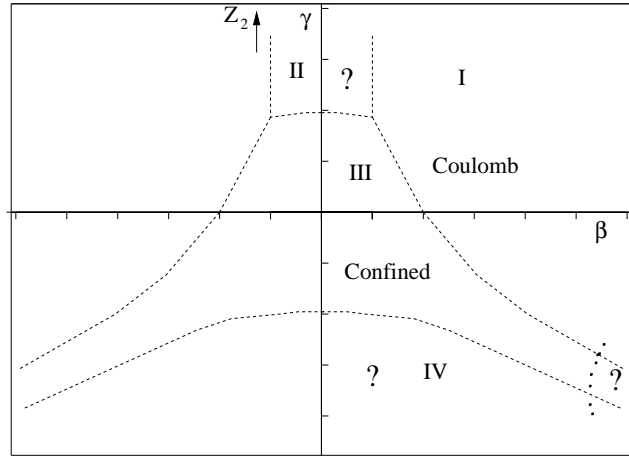


Figure 1: Phase diagram of the extended $U(1)$ model.

Three unknown aspects of the phase diagram are indicated with question marks:

1. the nature of the phase indicated with II ;
2. the nature of the phase IV ;
3. the fate of the two phase boundaries in the bottom right corner of the phase diagram (the same holds for the bottom left corner).

Another long standing question, still not completely resolved, is the order of the phase transition, especially along the $I - III$ line. A recent paper [11] shows, through a high statistics analysis of the plaquette action distribution, that the transition is first-order along the Wilson axis. We will confirm this result using a totally different observable. It is also numerically known that the transition becomes weaker and weaker as γ becomes negative, which motivated the hypothesis that a tricritical point could exist [12] along the phase boundary between regions I and III (see Fig. 1), beyond which the transition could be second-order. We will also address this issue with our new observable.

We now introduce the notion of flux, which will provide the tool we need to explore the phase diagram.

3 The flux in Abelian gauge theories

To introduce the notion of flux we need in $4d$, it is more natural to start from the $2d$ case. Consider a compact $U(1)$ gauge theory defined on a $2d$ lattice, with sizes L_μ, L_ν , and p.b.c.. Let us consider the definition

$$\Phi = \sum_P [\theta_P]_{-\pi, \pi} \quad (3)$$

where $[\theta_P]_{-\pi, \pi}$ is the plaquette angle reduced to the interval $(-\pi, \pi)$ (its so-called *physical* part), and the sum is over all plaquettes. This quantity, due to p.b.c., is $2\pi k$ valued ($k \in \mathbb{Z}$), because each link is summed twice with opposite signs, giving, overall, 0 modulo 2π .

If we consider the limit $a \rightarrow 0$, we obtain the standard result

$$\frac{1}{ea^2} (\theta_P)_{\mu\nu} \rightarrow F_{\mu\nu} = \partial_\mu A_\nu - \partial_\nu A_\mu \quad (4)$$

where $F_{\mu\nu}$ is the field strength; so the definition in Eq. (3) becomes

$$\frac{1}{e} \Phi_{\mu\nu} = \int F_{\mu\nu} d\sigma \quad (5)$$

which motivates the interpretation of Φ as an *e.m. flux*. Furthermore, in this limit we notice that fluxes corresponding to different values of k are *topologically* disconnected, in the sense that no tunneling is possible between two flux values through a smooth variation of gauge field. In fact, to change the value of the flux, one plaquette angle must exceed the value of π ; the statistical suppression of this change is $e^{-\beta\Delta S} \sim e^{-2\beta}$, which goes to zero in the continuum limit ($\beta \rightarrow \infty$).³

Consider now the same theory, but with $d = 4$. Call L_μ, L_ν, L_σ and L_ρ the four sizes of the lattice. Our definition of flux through any (μ, ν) orientation is:

$$\Phi_{\mu\nu} = \frac{1}{L_\rho L_\sigma} \sum_{\mu\nu \text{ planes}} \sum_{P_{\mu\nu}} [(\theta_P)_{\mu\nu}]_{-\pi, \pi} \quad (6)$$

A double sum is present:

- the *internal* $\sum_{P_{\mu\nu}}$ is the sum over the plaquettes in a single plane. So plane by plane we use the same definition as in the $2d$ case.
- the *external* average $\frac{1}{L_\rho L_\sigma} \sum_{\mu\nu \text{ planes}}$ over all parallel planes of a given orientation is non-trivial because the flux through different planes can change (in $3d$, for example, there are monopoles between planes). The allowed values for $\Phi_{\mu\nu}$ are thus multiples of $2\pi/L_\rho L_\sigma$.

Configurations whose flux is $2\pi k$ play a special role, for reasons which will be clear in the next section, and we say that they define *flux sectors*.

Let us compute the action of a flux sector in the *classical* (minimal action) limit. In this case the flux through a single plane is equally distributed over all plaquettes and it does not change across parallel planes:

$$(\theta_P)_{\mu\nu} = \frac{\Phi}{L_\mu L_\nu} = \frac{2\pi k}{L_\mu L_\nu}, \quad k \in Z \quad (7)$$

We obtain (here for the Wilson action)

$$S_k = 2\beta\pi^2 k^2 \frac{L_\rho L_\sigma}{L_\mu L_\nu} \quad (8)$$

showing that higher values of the flux are strongly suppressed. We stress that in the classical limit, even if $\Phi/2\pi$ is not integer valued because of the presence, e.g., of an external field, the action is anyway quadratic in the flux:

$$S = \frac{1}{2}\beta\Phi^2 \frac{L_\rho L_\sigma}{L_\mu L_\nu} \quad (9)$$

³In the $2d$ case the lack of ergodicity through flux values of simulations at large β can be cured by a cluster algorithm [13].

In all actual simulations we will work with hypercubic lattices, where $L_\mu = L \forall \mu$, so that the geometric factor $\frac{L_\rho L_\sigma}{L_\mu L_\nu}$ is 1.

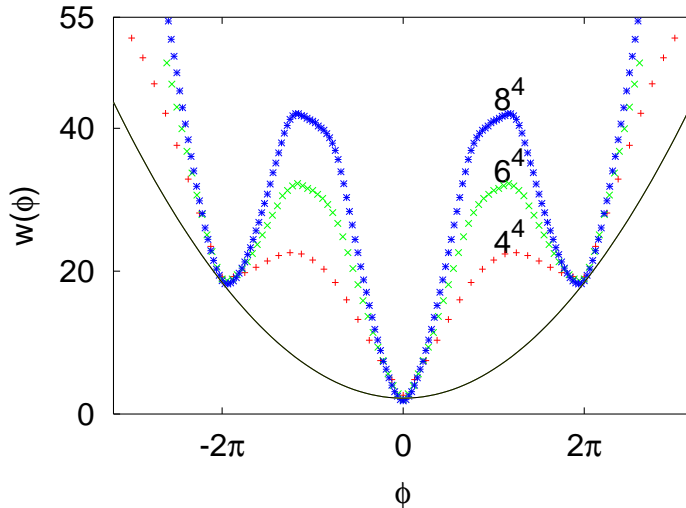


Figure 2: Flux effective potential in the Coulomb phase at $\beta = 1.2$ and $\gamma = 0$ (for lattice size $L = 4, 6, 8$). The dashed parabolic line is Eq. (9) with $\beta = 0.85$; for a discussion of this value see section 7.2.

4 Characterization of the phase transition

In this section we consider the behavior of flux sectors across a phase boundary. For this purpose we measure the *flux distribution* $\rho(\phi)$ through one (μ, ν) orientation during a Monte Carlo simulation. Since this quantity extends over several orders of magnitude, we will show the *flux effective potential* $w(\phi)$, defined by

$$\rho(\phi) = e^{-w(\phi)} \quad (10)$$

The results of our simulations are the following:

1. In the Coulomb phase we observe minima of the flux effective potential at flux values $2\pi k$ ($k \in \mathbb{Z}$) (Fig. 2). As the thermodynamic limit is approached we observe barriers of diverging height between those minima, while the flux effective potential at $2\pi k$ does not change. Extrapolating to the thermodynamic limit, we obtain that no tunneling is allowed between sectors: this property finally motivates the use of the word ‘sector’ we introduced at the beginning.

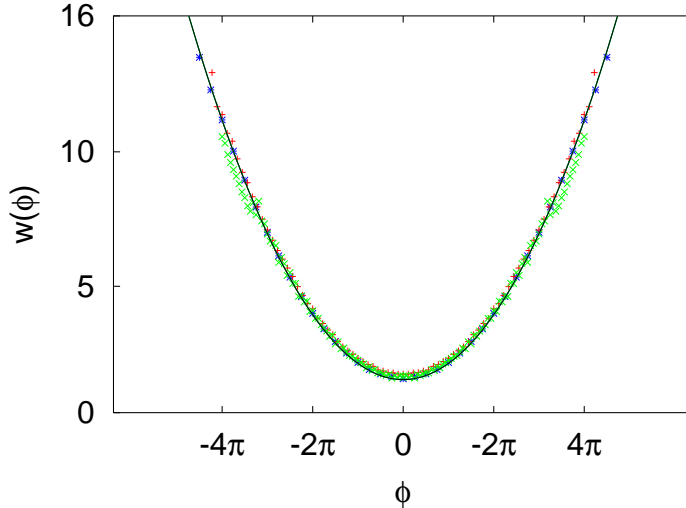


Figure 3: Flux effective potential in the confined phase at $\beta = 0.8$ and $\gamma = 0$ ($L = 4, 6, 8$). A parabolic interpolating curve is superimposed ($\rho(\phi) = e^{-\phi^2/2\sigma^2}$, $\sigma = 2.8$).

2. In the confined phase (Fig. 3) sectors are not defined, in the sense that no local minima of the flux potential are observed. The distribution of the flux values is continuous (in the limit $L \rightarrow \infty$), gaussian and independent of the lattice size.

From the point of view of the flux picture of the model, Figures 2 and 3 characterize completely the phase transition.

We now want to interpret all these results in terms of the monopole picture. We first discuss the interpretation of a *flux tunneling event* (in the Coulomb phase, when $L < \infty$, we observed that tunnelings across flux sectors are not forbidden, only suppressed). Let us start from the observation that monopoles are created in pairs and that a plane pierced by a Dirac string [4] gets an extra flux of 2π . Consider a monopole configuration of the kind shown in Fig. 4 where a monopole-antimonopole pair at a certain distance d wraps around the periodic boundaries; in Fig. 4 we show that a stack of d planes is pierced by a Dirac string. Let $d \rightarrow L_\mu$ (the lattice size): due to p.b.c. the two particles annihilate, and the configuration realized is the so-called *Dirac sheet*. This is the configuration responsible for a tunneling event; any other configuration produces a variation of flux only in a fraction of the planes, and thus is responsible for the non-integer (*mod* 2π) values of the flux.

In the Coulomb phase only a few, small loops are created, so it is very unlikely to have monopole lines wrapping around the boundaries. If the volume is finite, there is a finite probability p for this event to happen, which vanishes like e^{-L} as

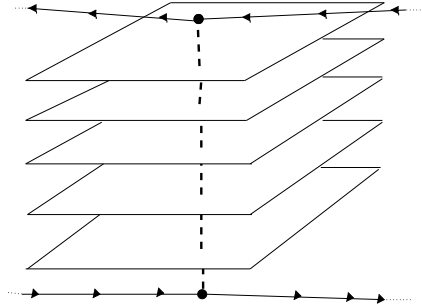


Figure 4: Monopole configuration corresponding to a flux tunneling event. The dashed line represents the Dirac string, the solid lines the monopole world-lines, wrapping around the boundaries.

$L \rightarrow \infty$, as one can observe in Fig. 2. The reason for this exponential decay is that a tunneling event is possible only in presence of two monopole loops of length L (wrapping loops), and the free energy cost of a loop is proportional to its length.

In the confined phase, instead, a large number of monopoles and percolating loops of arbitrarily large size are present, so that the flux values through different planes are totally *de-correlated*; the flux through one plane can be considered as a random variable with a given distribution. The same definition applied to another plane gives another *independent* random variable, with the same distribution. Therefore the total flux Eq. (6) is just the normalized sum of independent random variables, whose distribution is gaussian as $L \rightarrow \infty$. It is remarkable that also the smallest lattice we used ($L = 4$, that is, with 16 parallel planes in the μ, ν orientation) has the same distribution as the largest one, indicating that the central limit ‘converges’ quickly to its asymptotic distribution.

Moreover, the variance σ of the gaussian distribution is related to the density δ of monopole currents. Call f the fraction of monopoles which contribute to flux disorder. Then, between two successive planes, $L^2 f \delta$ monopoles contribute to flux change. If the global flux (averaged over L^2 planes) has variance σ^2 , the flux through one plane has variance $L^2 \sigma^2$ and the difference of flux between two planes has variance $2L^2 \sigma^2$. In this way we estimate

$$f \delta = 2 \left(\frac{\sigma}{2\pi} \right)^2 \quad (11)$$

where we divide σ by 2π to relate the units of flux ($\in 2\pi N$) to the number of monopoles ($\in N$) through which we define δ . Knowing σ (see caption of Fig. 3) and measuring $\delta = 0.488$, we estimate $f \sim 0.81$: the physical picture is thus that 80% of the monopoles contribute to flux disorder at $\beta = 0.8$. We checked that this result

context of $SU(N)$ pure gauge theories, we know that it is possible to modify the flux (by twisting the boundary conditions) according to the discrete group Z_N , center of $SU(N)$. This modification arises from the requirement of changing the boundary conditions of a gauge system defined on a hypertorus T^4 in the most general way compatible with gauge invariance. We can implement a similar change also in the Abelian context, but now the difference is that we can vary the flux *continuously*. For this reason we will intentionally use the word ‘twist’ as a synonym of ‘flux’.⁴

In order to implement this idea consider a stack of plaquettes, one in each plane of a given orientation, as indicated (for the 3d case) in Fig. 6, and change their value as:

$$\theta_P \rightarrow \theta_P + \phi, \quad \phi \in R \tag{12}$$

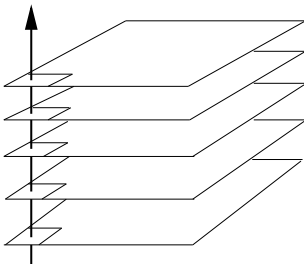


Figure 6: 3d representation of the ‘twists’ in $U(1)$ gauge theory. Each (μ, ν) plane now carries flux ϕ .

The new partition function is

$$Z(\phi) = \int D\theta e^{\sum_{stack} (\beta \cos(\theta_p + \phi) + \gamma \cos(2(\theta_p + \phi))) + \sum_{\overline{stack}} (\beta \cos \theta_p + \gamma \cos 2\theta_p)} \tag{13}$$

where *stack* indicates the set of plaquettes through which the extra flux is imposed. For instance

$$stack = \{\theta_{\mu\nu}(x, y, z, t) \mid \mu = 1, \nu = 2; x = 1, y = 1\} \tag{14}$$

\overline{stack} is its complement, that is all the other unchanged plaquettes. Observe that $Z(\phi)$ is clearly 2π periodic, so actually the flux we add to the system is defined only *mod* 2π . It is not manifestly translationally invariant, but it is easy to show that we can freely move the position of the stack through a redefinition of the link variables. In Fig. 7 we show a two-dimensional cartoon of this change of variables: u is a link, and ϕ inside the plaquette indicates the extra flux. A change $u \rightarrow e^{-i\phi}u$ moves

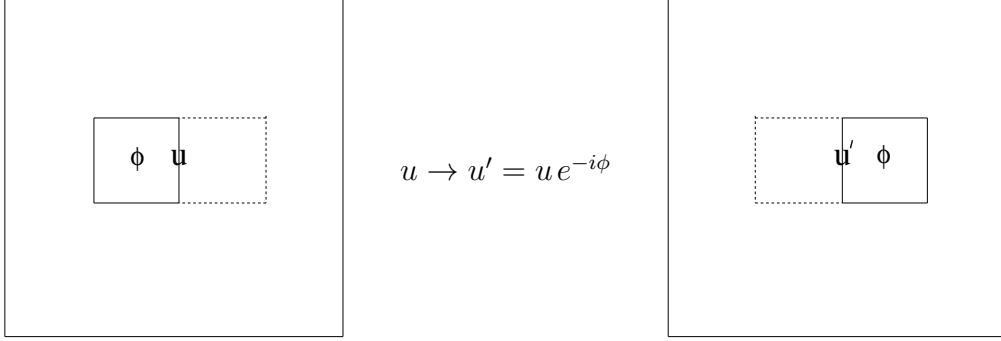


Figure 7: Graphical representation of the change of variables that moves the twisted stack. u indicates a link; ϕ is the twist imposed on the plaquette.

the stack to a neighboring position. With a similar transformation (namely, moving only part of the flux from the initial plaquette) one can spread the flux arbitrarily over several plaquettes, in particular, homogeneously through the whole plane.

Observe that we can implement the presence of an extra flux also in terms of *modified ("twisted") boundary conditions*

$$U_2(x + L_1, y = 1, z, t) = U_2(x, y = 1, z, t) e^{i\phi} \quad (15)$$

This remark will play an important role in the following.

We measure the free energy of the flux, defined by

$$F(\phi) = -\log \frac{Z(\phi)}{Z(0)} \quad (16)$$

and the results are as follows:

1. In the confined phase (Fig. 8, lowest curve), within our statistical error, the free energy is independent of ϕ . The reason for this phenomenon is clear from Eq. (15). Since the flux variation can be interpreted as a modification of the boundary conditions, we expect that in the confined phase the system is insensitive to them, because the correlation length ξ is finite (finite size corrections to $F(\phi)$ are $\mathcal{O}(e^{-L/\xi})$).
2. In the Coulomb (massless) phase the interaction is long-range and the system becomes sensitive to the boundary conditions (Fig. 8, upper curves).

⁴For an earlier, related study of compact $U(1)$ in an external field, see [16].

It is possible to describe this behavior in terms of classical arguments: we write the partition function of the system as a *sum over flux sectors* of the classical partition functions corresponding to each sector, as derived in Eq. (8)

$$Z(\phi) = \sum_k Z_{cl.}(\phi + 2\pi k) = \sum_k e^{-\frac{\beta_{\text{eff}}}{2}(\phi+2\pi k)^2} \quad (17)$$

We fit the flux free energy according to Eq. (17), letting β_{eff} be a free parameter. The good description of the data provided by this ansatz (see Fig. 8) motivates the interpretation of β_{eff} as an *effective* coupling, which takes into account the quantum fluctuations (that is, the contribution of the monopole excitations) of the system. In section 6 we will discuss this point in more detail.

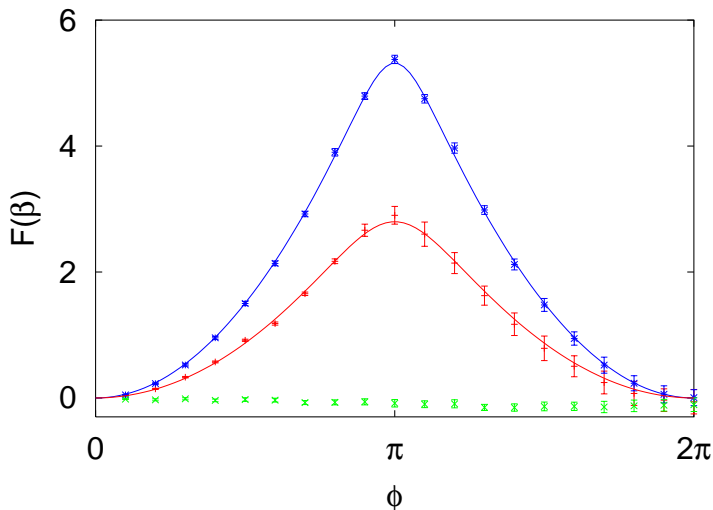


Figure 8: Free energy $F(\phi)$ in the Coulomb phase ($\beta = 1.5, 1.1$, upper and middle curve) and in the confined phase ($\beta = 0.8$, lower curve) (4^4 lattice). The fit by the ansatz Eq. (17) is superimposed to the data. The effective couplings in the Coulomb phase are $\beta_{\text{eff.}} = 1.2, 0.71$ respectively.

3. In the unknown phases *II* and *IV* we observe (within the statistical error) the appearance of an extra π periodicity (Fig. 9). We now propose an argument to interpret this finding.

Consider the following Polyakov loop correlator

$$\langle P_q(x) P_q^\dagger(x + L_\mu \hat{e}_\mu) \rangle_{\bar{Z}} \quad (18)$$

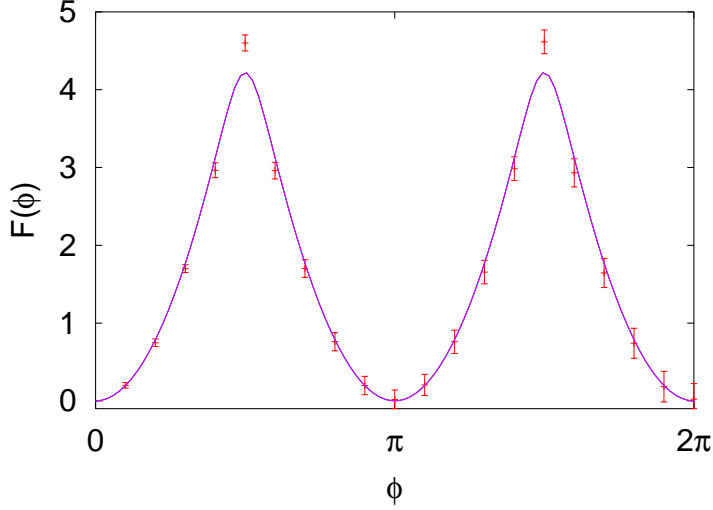


Figure 9: Typical free energy profile in phases *II* and *IV* ($\beta = 1.0$, $\gamma = -1.5$; 4^4 lattice). The fit by the ansatz Eq. (17) (with the change $2\pi \rightarrow \pi$) is superimposed (giving a value of $\beta_{\text{eff}} \sim 3.98$).

Here P_q is the Polyakov loop of charge q in direction $\hat{\nu}$

$$P_q(x) = e^{iq \sum_{l=1}^L \theta_\nu(x+l\hat{e}_\nu)} \quad (19)$$

We take the average w.r.t. $\tilde{Z} = \int_0^{2\pi} d\phi Z(\phi)$, in order to implement the influence of all possible external fluxes (*mod* 2π) on the system; the physics anyway does not change. Even though the correlator is measured between point x and its periodic image $x + L_\mu \hat{e}_\mu$, it is non-trivial due to the 'twisted' b.c. (Eq. (15)). Gauss law gives

$$P_q(x + L_\mu \hat{e}_\mu) = e^{-iq\phi} P_q(x) \quad (20)$$

that is the two Polyakov loops differ by the flux we added. Inserting this relation in Eq. (18) we get

$$\langle P_q(x) P_q^\dagger(x + L\hat{e}_\mu) \rangle_{\tilde{Z}} = \frac{\int_0^{2\pi} d\phi e^{iq\phi} Z(\phi)}{\int_0^{2\pi} d\phi Z(\phi)} \quad (21)$$

If $Z(\phi)$ has periodicity π , it follows that when $q = 1$, or more generally odd, the numerator vanishes and the correlator is zero, while if q is even, it can be different from zero. Noting that

$$\langle P_q(x) P_q^\dagger(x + L_\mu \hat{e}_\mu) \rangle \sim e^{-V_q(L_\mu)L_\nu} \quad (22)$$

where V_q is the static potential between the static charges $\pm q$ represented by the Polyakov loops, a vanishing Polyakov loop correlator implies an infinite (confining) potential.

We therefore claim that the two unknown phases II and IV are just Coulomb phases for *even* electric charges, while odd charges are confined and paired in even combinations.

Maybe a simpler argument can start from the observation that this result is trivially true in the Coulomb phase along the axis $\beta = 0$, where the π periodicity is a simple consequence of the symmetry $(\beta, 0) \rightarrow (0, \beta)$ discussed in Sec. 2. It then easily extends to the whole regions II and IV of Fig.1, since a phase is characterized by a given infra-red (IR) behavior. Indeed our numerical results (obtained at $\beta = 1.0$ and $\gamma = -1.5$) (Fig. 9) show no detectable deviation from π periodicity.

The extra periodicity is also a useful tool to discuss the fate of the two phase boundaries at the lower corners of Fig. 1. It is possible that these phase boundaries meet at some point or that they just become asymptotically close to each other. What we can exclude is that they meet and terminate somewhere, letting the two different Coulomb phases communicate. Suppose that they communicate somewhere, then we expect the twisted free energy $F(\phi)$ (Fig. 8 and 9) to be the same in both: but this leads to a contradiction. In fact $F(\phi)$ would have *least* periodicity π and 2π at the same time. This is only possible if the distribution is flat, which only happens in the confined, not the Coulomb, phase.

We conclude this section with some comments about the numerical strategy used to compute the free energy Eq. (16). Here we are faced with an *overlap* problem, that is, in the ratio $\frac{Z(\phi)}{Z(0)}$, the numerator and the denominator sample non-overlapping regions of the configuration space. We can cure this situation through the following strategy [17]. Divide the interval $[0, 2\pi)$ into N parts, and consider the identity

$$\frac{Z(2\pi)}{Z(0)} = \frac{Z_N}{Z_{N-1}} \frac{Z_{N-1}}{Z_{N-2}} \dots \frac{Z_1}{Z_0} \quad (23)$$

where Z_k is defined as the partition function of a system with an extra flux $\phi = \frac{2\pi}{N}k$. We observe that for each ratio the overlap between numerator and denominator is much better now. A further improvement of the overlap (and, therefore, further variance-reduction) is obtained if we express each ratio as

$$\frac{Z_k}{Z_{k-1}} = \frac{Z_k/Z_{k-\frac{1}{2}}}{Z_{k-1}/Z_{k-\frac{1}{2}}} \quad (24)$$

where the index $k - \frac{1}{2}$ refers to an external flux $\phi = (k - \frac{1}{2}) \frac{2\pi}{N}$. The numerator and

the denominator of each ratio are ratios themselves, where, for example,

$$\frac{Z_k}{Z_{k-\frac{1}{2}}} = \langle e^{-(S_k - S_{k-\frac{1}{2}})} \rangle_{Z_{k-\frac{1}{2}}} \quad (25)$$

S_k is the action of the system when an external flux $k \frac{2\pi}{N}$ is added. This ratio can be directly computed. The algorithm consists of measuring all these ratios separately and recombining them according to Eqs. (23)(24). It is a trivial matter to extract statistical errors since the N ratios are estimated by independent Monte Carlo simulations.

6 The helicity modulus

We now go back to Fig. 8, i.e., to the free energy of a system with twist ϕ . Consider the *curvature* of the free energy profile at some arbitrary value of the flux $\phi = \bar{\phi}$. In the confined phase it is identically zero (in the thermodynamic limit), because of the independence of $F(\phi)$ from ϕ . In the Coulomb phase this quantity is different from zero. Therefore there is certainly a point of non-analyticity for this quantity at the transition: it is an *order parameter*.

We are then motivated to introduce the following definition

$$h(\beta, \gamma) = \left. \frac{\partial^2 F(\phi)}{\partial \phi^2} \right|_{\phi=\bar{\phi}=0} \quad (26)$$

known as the *helicity modulus* in the literature [1] [2] (we stress that the choice $\bar{\phi} = 0$ is arbitrary). This name was conceived in the context of the XY (rotor) model, where the boundary conditions are changed by adding an angle ϕ to the rotor phase $\theta(x, y)$ [2]

$$\theta(x + L_1, y) = \theta(x, y) + \phi \quad (27)$$

so that the quantity (26) assumes the meaning of the response function (‘modulus’) to a rotation (‘helicity’) of the boundaries. Eq. (27) is the analog of Eq. (15) in our case.

If we substitute our partition function $Z(\phi)$ Eq. (13) into Eq. (26) we obtain the following expression

$$h(\beta, \gamma) = \left\langle \sum_{stack} (\beta \cos[\theta_P] + 4\gamma \cos[2\theta_P]) \right\rangle - \left\langle \left(\sum_{stack} (\beta \sin[\theta_P] + 2\gamma \sin[2\theta_P]) \right)^2 \right\rangle \quad (28)$$

where ‘*stack*’ refers to the stack of plaquettes we changed by adding the flux (see Section 5). As we noted earlier, we are allowed to spread the flux homogeneously

through the planes via a coordinate transformation. If we add to each plaquette of a given orientation the flux $\phi/L_\mu L_\nu$ and recompute Eq. (26), we obtain equivalently

$$h(\beta, \gamma) = \frac{1}{(L_\mu L_\nu)^2} \left\{ \left\langle \sum_P (\beta \cos[\theta_P] + 4\gamma \cos[2\theta_P]) \right\rangle \right. \\ \left. - \left\langle \left(\sum_P (\beta \sin[\theta_P] + 2\gamma \sin[2\theta_P]) \right)^2 \right\rangle \right\} \quad (29)$$

where now the sum extends over all plaquettes in the (μ, ν) orientation. This expression turned out to give a much smaller variance than the other one.

Suppose that $\gamma = 0$. Then it is interesting to observe that in the confined phase, where this order parameter is zero, the average action (first term) is related to a measure of its fluctuations (second term).

7 Helicity modulus: numerical results

We now present the results of a numerical study of the helicity modulus. First, in Fig. 10, we show the behavior of this quantity on the Wilson axis. Remaining for the moment on a qualitative footing, we see that it indeed behaves like an order parameter. On the extended line ($\beta = 0$) we would obtain the same plot up to a factor 4, as is clear looking at Eq. (28) and remembering the symmetry $(\beta, 0) \leftrightarrow (0, \beta)$ of the partition function $Z(\beta, \gamma)$.

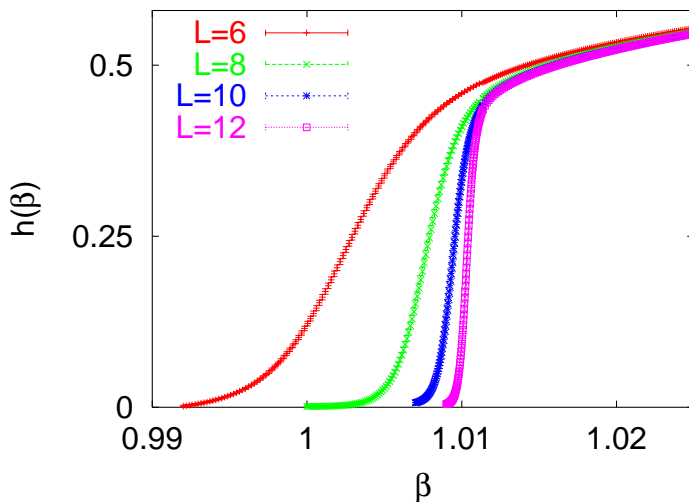


Figure 10: Helicity modulus on the Wilson axis near the phase transition.

The statistics used for this measurement is of about 10^5 measurements per lattice size, with one heatbath and four overrelaxation sweeps between two subsequent measurements. The curves in Fig. 10 are obtained through a reweighting of the data *à la* Ferrenberg-Swendsen [18].

Let us now consider the behavior of the helicity modulus in the whole phase diagram. Again refer to Fig. 1, fix the value of $\beta = 2.50$, for example, and consider the (negative) values of γ in a region across the phase boundaries of the diagram. We show the result in Fig. 11. Also in this case the expectations are qualitatively satisfied: the flat region signals the presence of a confining phase, and the helicity modulus is roughly 4 times higher in the even-charge Coulomb phase than in the other one.

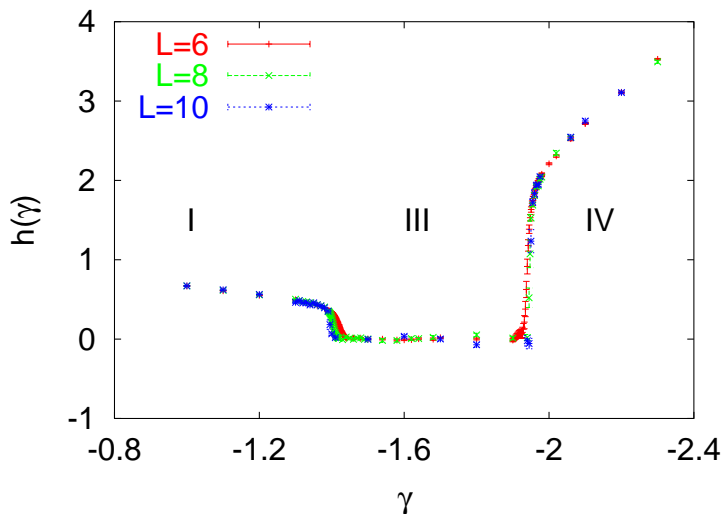


Figure 11: Helicity modulus versus γ ($\beta = 2.5$ fixed; $L = 6, 8, 10$). Label ‘*I*’ indicates the usual Coulomb phase, ‘*III*’ the confined phase, ‘*IV*’ the even-charge Coulomb phase.

From the numerical point of view, even if the statistics used is roughly the same as on the Wilson axis (at least across the phase transitions), these data are less accurate than the other ones: at such a small coupling the Monte Carlo dynamics is slower (much larger autocorrelation time).

In the next sub-sections we perform a quantitative analysis of these data, in order to clarify the issues of the order of the phase transition, of the relation between the helicity modulus and the renormalized coupling, and finally of the conjectured universality of the helicity modulus at β_c [2].

7.1 Order of the phase transition

The difficulty of determining the order of a phase transition using lattice simulations is well known, and, in general terms, is due to the fact that in finite systems no singularities of the free energy can be present. In our specific case we are interested in distinguishing a first- from a second-order transition, but we know that even in the first-order scenario the correlation length ξ_c at the transition point can be quite large, so that for lattices of size $L \lesssim \xi_c$ the transition mimics a second-order one. This can explain the difficulty that was encountered in solving this problem so far.

As shown in Fig. 10 the finite-size (FS) effects act to round off the singularity into smooth curves. It turns out that their functional form depends on the *order* of the phase transition, so that an ansatz for the FS effects, when available, provides a direct way to prove or disprove a conjecture about the nature of the phase transition. Since we have accurate data for the helicity modulus for lattices of size up to $L = 14$, we try to make such an analysis both for the first- and the second-order scenarios.

From a theoretical point of view, little is known about the order of the transition. If the correlation length would diverge at the transition point (as happens in the second-order scenario), it would be possible to extract a continuum limit, leading to a continuum *confining Abelian* theory, which seems unlikely. From a numerical point of view, a quite recent study [11] of the $4d$ Abelian Wilson action strongly supports the first-order scenario, through a high statistics analysis of the action density distribution (considering lattices of size up to $L = 18$).

Let us first consider the first-order scenario, and make the hypothesis that the helicity modulus has a *jump* across the transition point. We now consider the simplest ansatz for the partition function in the vicinity of the transition point

$$Z \sim e^{-Vf_-(\beta)} + Xe^{-Vf_+(\beta)} \quad (30)$$

where f_- , f_+ denote the free energy densities of the two coexisting phases (such that $f_-(\beta_c) = f_+(\beta_c)$), and X is the so-called *phase asymmetry parameter*, that is the relative weight of the two phases at the coexisting point. Eq. (30) is the Borgs-Kotecky ansatz [19][20], but we have to observe that the work of these two authors is based on a Peierls-like contour picture of the system at the transition point, with the hypothesis that the contours (that is, the boundary of domains characterized by a single phase) do not interact with each other. The long-range nature of the photon interaction in the Coulomb phase makes it difficult to justify such a hypothesis. A posteriori, we will indeed observe deviations from the predictions based on this ansatz: for example, finite-size corrections to the fitting parameters different from the standard ones proportional to $\frac{1}{V}$ will be necessary.

The ansatz of Eq. (30) leads to a formula for the interpolating FS curves which we write in the following way

$$h(\beta, V) = \frac{h_+}{1 + X^{-1}e^{-V\Delta f' \cdot (\beta - \beta_c)}} \quad (31)$$

where h_+ is the value of the helicity modulus in the pure Coulomb phase (see Fig. 13), and $\Delta f' = f'_+ - f'_-$ is the *latent heat*, obtained from the expansion

$$f_{\pm}(\beta) = f_c + f'_{\pm} \cdot (\beta - \beta_c) + \mathcal{O}(\Delta\beta^2). \quad (32)$$

Since for simplicity h_+ is taken as constant in the Coulomb phase, the purpose of the ansatz is to describe the helicity modulus just below the transition, and we perform a fit for values of $\beta \leq \beta_c$ (actually the range was limited to an interval $[\beta_1, \beta_c]$, with β_1 close to β_c , to take into account the approximation introduced by linearizing Eq. (32)). For β_c we use the very precise value in [11], and also we determine it self-consistently from the fit of our data (iteratively, we fit the data in an extended β range, determine β_c and make another fit in a range up to the new value; we repeat this procedure until β_c stabilizes). An analysis of the possible FS corrections indicates that a minimal choice is the following

$$h_+ \rightarrow h_+ \cdot \left(1 + \frac{\alpha_1}{L}\right) \quad (33)$$

$$\Delta f' \rightarrow \Delta f' \cdot \left(1 + \frac{\alpha_2}{V}\right) \quad (34)$$

For the *latent heat* we consider $1/V$ corrections, standard for a first-order transition. To justify the $1/L$ corrections used for h_+ , first let us look at the behavior of the helicity modulus at the transition point (Fig. 12).

We fit these data with the ansatz

$$h_c(L) = h_c(\infty) \cdot \left(1 + \frac{c}{L^\nu}\right) \quad (35)$$

where c is a constant, and obtain the result $\nu = 1.04(12)$, which is a first numerical indication for the choice of the FS correction Eq. (33). At the end of this paragraph we are going to comment more extensively about this choice. Then, fixing $\nu = 1$, we get the thermodynamic value $h_c(\infty) = \frac{h_+}{1+X^{-1}} = 0.371(1)$ ($c = 1.7$), independently from the Borgs-Kotecky ansatz. This value is only slightly increasing if we exclude from the fit the points corresponding to $L = 4, 6$.

We then turn to the ansatz Eq. (31) and fit the data corresponding to lattices $L = 8, 10, 12, 14$, obtaining the following results:

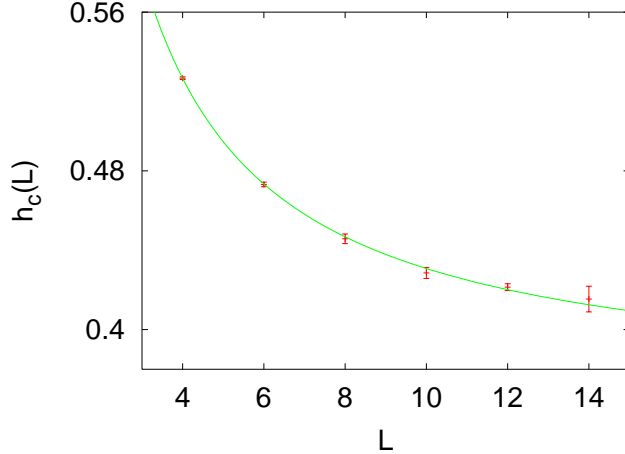


Figure 12: Helicity modulus at the transition point versus lattice size.

$$h_+ = 0.381(5) \quad (36)$$

$$\Delta f'/6 = 0.029(2) \quad (37)$$

$$\log X = 3.20(15) \quad (38)$$

$$\beta_c = 1.01108(5) \quad (39)$$

$$\alpha_1 \simeq 1.8 \quad (40)$$

$$\alpha_2 \simeq (3.7)^4 \quad (41)$$

Comparing the quantities β_c , $\log X$ and $\Delta f'/6$ (the latent heat per plaquette) with earlier measurements by Arnold et al. [21][11], the agreement is very good for all the values.

As a crosscheck, we can relate the value of $h_c(\infty) = 0.371(1)$ measured before, and $h_+ = 0.381(5)$ in Eq. (36). Their physical meaning is explained in Fig. 13: h_+ is defined as

$$h_+ = \lim_{\beta \rightarrow \beta^+} h(\beta) \quad (42)$$

and its value depends on the Coulomb phase only, while h_c is smaller, and takes into account the coexisting confined phase. As one can easily check, the relation

$$h(\beta_c) = \frac{h_+}{1 + X^{-1}} \quad (43)$$

(Eq. (31) computed at $\beta = \beta_c$) is consistent with our numerical values.

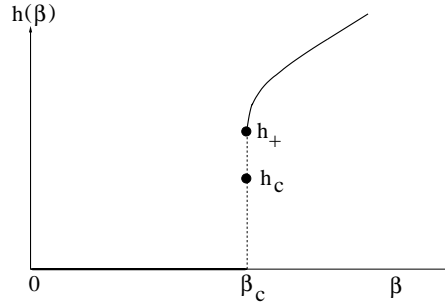


Figure 13: Graphical explanation of the physical meaning of the parameters h_+ and $h_c \equiv h(\beta_c, V = \infty)$, as defined in Eq. (31).

We also measured the value of h_+ directly, extracting from the canonical ensemble at β_c the subset of configurations whose action density is lower than a threshold value (0.359) chosen to best separate the two phases; in this way one can probe the Coulomb phase contribution only. We find $h_+ = 0.4325(15)$, a value incompatible with the value fitted using the BK ansatz. The discussion of this problem is postponed to the end of this section.

All the errors are computed performing a jackknife analysis. The values of α_1, α_2 are mentioned, to give an idea of the magnitude of the correction involved. Since we want to show the relative correction that they induce, α_2 (which has dimension L^4) is expressed as a fourth power. To evaluate the quality of the fit we could not use just the reduced χ^2 , because the data we fit are re-weighted, so that the number of points in the fit and their mutual correlation play a role which is not properly taken into account by the value of χ^2 . So we decided to show directly a plot (Fig.14, left) of the fitted data. The most important signature of the first order nature of the transition is the exponential (and not power law) behavior of the helicity modulus as a function of the distance from the transition point, which is visible in the linear behavior (in log-scale) away from β_c (see Fig. 14).

Now, for completeness, we want to compare the quality of this ansatz with that of the second-order one. If the transition would be second-order, all quantities (in the vicinity of the critical point) should satisfy the scaling hypothesis, that is they should be a function of L/ξ (ξ is the correlation length) only. Since

$$\xi \sim (\beta - \beta_c)^{-\nu} \quad (44)$$

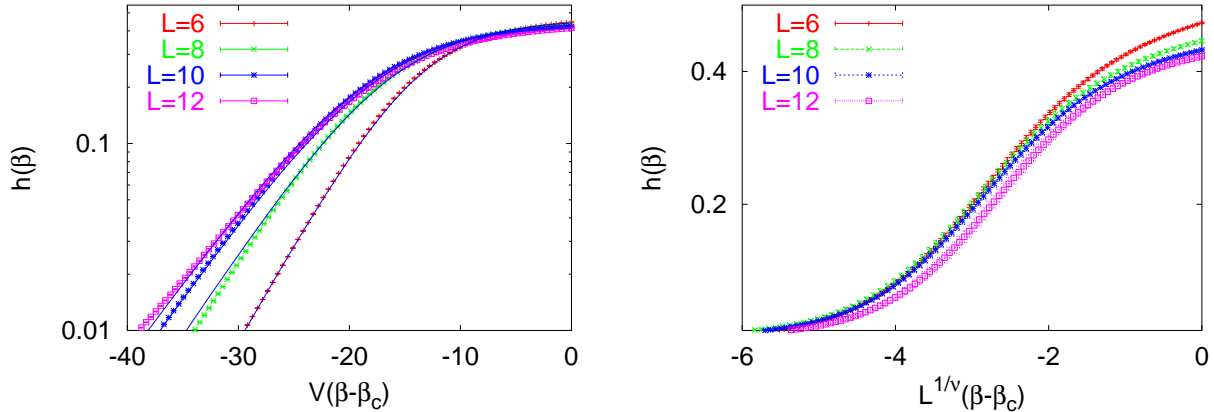


Figure 14: Graphical comparison of the quality of the first and second order ansatz for the helicity modulus data. The solid lines (left) show the first-order fit Eq.(31).

a rescaling of β according to

$$\beta \rightarrow L^{1/\nu}(\beta - \beta_c) \quad (45)$$

should produce a superposition (‘collapse’) of the data. The result of this analysis is shown in Fig. 14 on the right for the ‘test’ value of $\nu = 0.3$. The data collapse is quite poor: we consider this as an indication that the second-order scenario can be excluded.

We conclude this section with a discussion of the inconsistency we found between the determinations of h_+ using the BK ansatz ($h_+ = 0.381(5)$) and the direct measurement ($h_+ = 0.4325(15)$). On one hand, both methods are affected by systematic errors. Concerning the direct measurement, notice that a single metastable phase is not really a pure phase, but contains small ‘bubbles’ of the other one; furthermore the method is sensitive to the threshold value, which is chosen somewhat arbitrarily between the two peaks of the action density distribution. However, these two kinds of error diminish as the thermodynamic limit is approached; thus we were led to complement the other simulations with one on a large lattice (32^4) in order to consider these errors as small. Let us now scrutinize the BK ansatz. First of all we can consider the possibility that the lattices we used are too small, so that significant higher order $1/L^k, k > 1$ corrections should be added to the leading terms; but if we exclude from the fit the smallest lattices ($6^4, 8^4, 10^4$), no clear increase in the fitted value of h_+ is observed. Similarly, no clear change in the value of the fitting parameters occurs if we include a FS correction for X , the phase asymmetry parameter, not considered in Eqs. (33)(34). It appears that the BK ansatz does not describe so well the data very near the transition. The reason should be found, as we already

mentioned, in the long-range nature of the photon interaction, which is not taken into account by this ansatz based on a strong first-order picture. Note that corrections of order up to $1/V^4$ were found necessary in [11] to describe the behavior of the pseudocritical $\beta_c(L)$ on lattices of similar sizes to ours. From this discussion we also obtain some plausible motivation for the unusual FS correction ($1/L$ instead of $1/V$ at the leading order (Eq.(33))) we observe for the helicity modulus at the transition; we can impute such large correction to the interacting interfaces between the coexisting phases.

Therefore, we blame our inconsistency between the fitted and the measured value of h_+ on the limitations of the BK ansatz. The direct measurement of h_+ is independent of any specific model of the system at the transition, and the systematic errors that affect its value are certainly decreasing as the thermodynamic limit is approached. Thus, whenever possible, we will use this determination.

7.2 The helicity modulus and the renormalized coupling

We now want to discuss a remarkable property of our order parameter [2]: the helicity modulus in the Coulomb phase is related to the value of the renormalized coupling. Let us go back to the classical Eq. (9)

$$F(\phi) - F(0) = \frac{\beta}{2} \phi^2 \frac{L_\rho L_\sigma}{L_\mu L_\nu} \quad (46)$$

where, as already defined, $F(\phi)$ is the flux free energy. Following [2] we can define a so-called ‘blocking transformation’. As the number of RG steps increases and short distances are integrated out, only one relevant, Coulombic coupling survives, while all other couplings go to zero. In this way, starting from Eq. (46), we end up with the result

$$F(\phi) - F(0) = \frac{\beta^R}{2} \phi^2 \frac{L_\rho L_\sigma}{L_\mu L_\nu} \quad (47)$$

where the bare coupling has been substituted by the renormalized one, but no other changes occurred. The second derivative of this quantity thus gives the renormalized coupling, as anticipated.

The next step is to observe that the functional form of Eq. (47) is not totally consistent: this equation does not present any periodicity in ϕ , but we know that the flux free energy is 2π periodic in ϕ , the external flux we add, as already visible in Eq. (13). Therefore we have to consider the influence of all the other flux sectors, according to Eq. (17), and write

$$F(\phi) = -\log\left(\sum_k e^{-\frac{\beta^R}{2} \cdot (\phi + 2\pi k)^2}\right) \quad (48)$$

which correctly displays the periodic structure of the flux free energy. In Fig. 15 we show a cartoon comparison of equations (47) and (48).

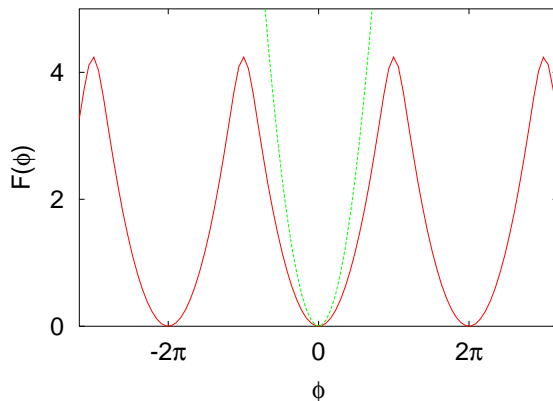


Figure 15: Qualitative behavior of the ansatz Eq. (48) and Eq. (47); the difference disappears in the limit $\beta \rightarrow \infty$.

Therefore we define $\beta_R(\beta)$ implicitly through the equation

$$\frac{\partial^2 F(\phi, \beta_R)}{\partial \phi^2} \Big|_{\phi=0} = h_0(\beta) \equiv h(\beta) \quad (49)$$

where $F(\phi, \beta)$ is given in Eq. (48). In order to give an idea of how the map $\beta_R(\beta)$ works, observe that in the limit $\beta \rightarrow \infty$ the following result holds

$$\beta_R(\beta) = \beta \left[1 - \frac{1}{4\beta} + \mathcal{O}\left(\frac{1}{\beta^2}\right) \right] \quad (50)$$

because as $\beta \rightarrow \infty$ the renormalized coupling is equal to the helicity modulus up to exponentially small corrections, hence we can use the weak coupling expansion of Sec.7.3.

In section 5 we already showed that the ansatz Eq. (48) provides an accurate description of the numerical data. Here we make a more refined check: this ansatz has to provide the right mapping between the helicity modulus at flux $\phi = 0$ and $\phi = \pi$. Since it depends on only one parameter, once the curvature at the origin is fixed, the curvature at $\phi = \pi$ has to be fixed too. In Table 1 we check the validity of this assumption. As we can see, the ansatz works very well over a wide range of β values. We also observe that from the theoretical point of view, defining the helicity modulus as the curvature of the flux free energy at flux π , instead of at flux

β	$h_{\phi=0}(\beta)$	$\frac{d^2 F}{d\phi^2}(\beta) _{\phi=\pi}$ derived from col.2	$h_{\phi=\pi}(\beta)$ measured
1.02	0.524(1)	-2.18(1)	-2.16(1)
1.10	0.713(1)	-4.30(1)	-4.30(1)
1.20	0.852(1)	-6.31(1)	-6.32(1)
1.30	0.972(1)	-8.35(2)	-8.32(1)

Table 1: Check of the validity of the ansatz Eq. (48). The first column is the bare (inverse) coupling; the second column is the measured value of the helicity modulus at flux 0; the third and the fourth columns correspond, respectively, to the analytic prediction of the helicity modulus at flux π , derived from that at flux 0 according to Eq. (49), and to the directly measured quantity (the measurements are made on a 10^4 lattice).

0, could have been a perfectly consistent choice:

$$\frac{\partial^2 F(\phi, \beta_R)}{\partial \phi^2} |_{\phi=\pi} = h_\pi(\beta) \quad (51)$$

Therefore, Eq.(51) provides an equivalent way to compute the renormalized coupling. Moreover, the data obtained at flux π are statistically more accurate.

We measured the two helicity moduli (at flux 0 and π) at $\beta = \beta_c^+$, in the Coulomb phase, on a 32^4 lattice, obtaining $h_{0,+} = 0.4325(15)$ and $h_{\pi,+} = -1.413(16)$ respectively. Then, we extracted the renormalized coupling from Eqs. (49) and (51). This gives

$$e_R^2 = \frac{1}{\beta_R} = 2.30(1) \quad \text{for } \phi = 0 \quad (52)$$

$$e_R^2 = \frac{1}{\beta_R} = 2.31(1) \quad \text{for } \phi = \pi \quad (53)$$

which are in agreement (on smaller lattices the renormalized coupling at flux zero is systematically smaller than the one at flux π ; one could use this difference as a criterion to evaluate how close to the thermodynamic limit we are.). We take as our final value the average, with a conservative error sufficient to cover both determinations:

$$e_R^2 = 2.305(15) \quad (54)$$

This value can be compared with those in the literature (up to a 4π factor) $e_R^2 = 2.08(14)$ [22] and $e_R^2 = 2.39(12)$ [23]. Our value is more accurate. The main

reason is that the other authors compute e_R^2 from a fit of the static potential between two charges, obtained from Wilson loops measurements; the limitations in the size of the loops makes the estimate more difficult. In our case, instead (see Eq. (29)), we do not have this limitation and use the lattice in its whole extension.

We can now go back and consider the analysis performed in the caption of Fig. 2. The parabolic curve, computed at flux $\phi = \pm 2\pi$, gives the classical suppression of the corresponding flux sectors. But a renormalized β appears in front of it: the value $\beta_{\text{eff.}} = 0.85$ was computed through the requirement that the parabola had to pass through the local minima. Instead, from a measurement of the helicity modulus at $\beta = 1.2$ one finds $\beta_R = 0.852(2)$. This perfect consistency is yet another check of the validity of Eqs.(47,48).

7.3 Universality of the helicity modulus

In [2] Cardy made a conjecture about the universality of the helicity modulus (that is, of the renormalized coupling) at the transition point. In the typical renormalization group language, ‘universality’ means that we are going to find the same value in all Abelian theories that share the same ‘long range’ properties, when approaching the boundary with the confined phase from the Coulomb side.

This conjecture is motivated by the formal analogies existing between the $4d$ compact $U(1)$ theory and the $2d$ XY model. Let us start by recalling the hamiltonian of the lattice $2d$ XY model

$$\mathcal{H} = -\rho \sum_{\langle ij \rangle} \cos(\theta(r_i) - \theta(r_j)) \quad (55)$$

where ρ is the coupling parameter (which has dimension of energy), $\theta(r_i)$ is the spin angle at site r_i , and the sum is over first neighbors. This leads, in the continuum, to

$$\mathcal{H} = \frac{1}{2} \int d^2x \rho (\nabla\theta(\vec{x}))^2 \quad (56)$$

and in this context ρ is called the *helicity modulus* (in analogy with what we did in the previous section, one can argue that there is a difference between the bare ρ , which is just a coupling constant, and the renormalized ρ_R , which takes into account the fluctuations of the system).

The partition functions of both theories admit a decomposition of the form [1],[5]

$$Z = Z_P Z_I \quad (57)$$

where Z_P is the partition function of a gas of massless excitations (spin waves for the XY model and photons – hence the subscript P – for $U(1)$) and of interacting – hence the subscript I – topological excitations (vortices for the XY model and monopole current loops for $U(1)$) interacting via a Coulombic potential.

Cardy then develops an analogy between the critical exponent η of the $2d$ XY model, characterizing the falloff of the spin-spin correlator (in the massless, large- β phase)

$$\langle e^{i\theta(r_1)} e^{-i\theta(r_2)} \rangle \sim |r_1 - r_2|^{-\eta} \quad (58)$$

and the renormalized coupling for the Abelian theory: both quantities arise from the additive renormalization of the bare coupling by the susceptibility of the topological defects

$$2\pi\eta = \frac{1}{\beta} - \pi^2 \sum_r (r/a)^2 \langle m(0)m(r) \rangle_I \quad (59)$$

$$\frac{1}{\beta^R} \equiv e_R^2 = \frac{1}{\beta} - \frac{\pi}{24} \sum_{r,\mu} (r/a)^2 \langle m_\mu(0)m_\mu(r) \rangle_I \quad (60)$$

where m represents the defect field, β is the bare coupling and the index I in $\langle \cdot \rangle_I$ represents the interacting part Z_I of the partition function in Eq. (57). The crucial step is to show the universality of η in the XY model. Computing explicitly the left side of Eq. (58) [7], one finds that

$$\eta = \frac{k_B T}{2\pi\rho} \quad (61)$$

where k_B is the Boltzmann constant, which provides a relation between η and the helicity modulus. Taking the limit $T \rightarrow T_c^-$ we find $\eta_c = \frac{1}{4}$: this result is independent of the specific RG trajectory considered, and therefore is *universal*, in the sense that it is unchanged when the short range features of the theory are modified. The combination of this result with the similarity between Eqs. (59) and (60) is the basis for Cardy's conjecture that e_R^2 is a universal quantity for the $4d$ Abelian theory.

The check of this hypothesis can be performed on different levels. To get a first qualitative idea of the analogy between the two theories we plot the quantity $\frac{h(\beta)}{\beta}$ of the $4d$ theory (Fig. 16), which can be compared directly with the helicity modulus in the XY model (our definition of the helicity modulus for $U(1)$ includes an extra factor β). In the XY model, the behavior near $T = 0$ is given by $(1 - \frac{1}{4}T)$, and approaching T_c^- by a power-law singularity $(h_c(1 + \frac{1}{2}(1 - \frac{T}{T_c})^\nu + \mathcal{O}(1 - \frac{T}{T_c})))$, $\nu = 0.5$) [7].

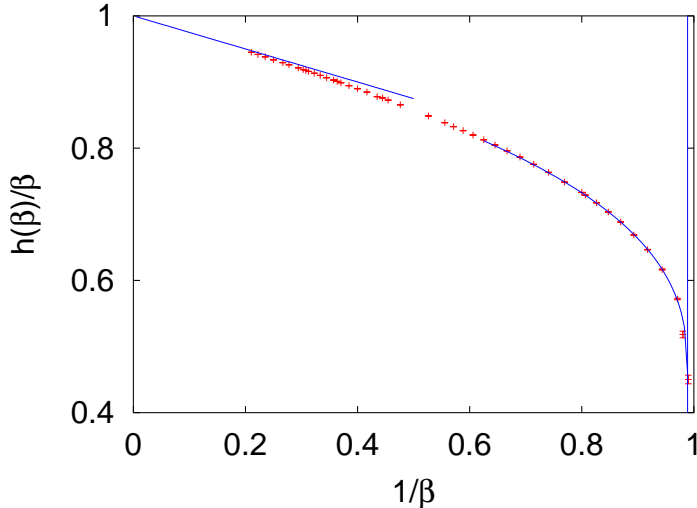


Figure 16: Helicity modulus in the $4d$ $U(1)$ theory (6^4 lattice), divided by β for direct comparison with the helicity modulus in the $2d$ XY model, as a function of “temperature” $1/\beta$. The linear and the power law expansions are represented around the regions $1/\beta \sim 0$ and, respectively, approaching the transition. The vertical line represents the transition point.

Considering the $U(1)$ case, we obtain the same behavior $\frac{h(\beta)}{\beta} = 1 - \frac{1}{4\beta} + \mathcal{O}(\frac{1}{\beta^2})$ from a weak coupling expansion⁵. Secondly, we measure the exponent ν from the ansatz

$$\frac{h(\beta)}{\beta} = \frac{h(\beta_c^+)}{\beta_c} \left(1 + \alpha \left(1 - \frac{\beta_c}{\beta}\right)^\nu\right) \quad (62)$$

close to the transition. The resulting exponent grows systematically with the lattice size, as shown in Tab. 2. From a full jackknife analysis of the data on our largest lattice ($L = 12$), we obtain $\nu = 0.34(3)$. This value compares well with the value $\nu = 0.43 \pm 0.10$ in [22], computed using the same ansatz for the renormalized coupling data (extracted from Wilson loops) in the vicinity of β_c . It is not excluded that the value 0.5 is attained, as in the XY model, in the thermodynamic limit. The overall agreement between the helicity modulus in the two theories is remarkable, and poses the issue of the universality of the jump of the order parameter at the transition on a more intuitive basis.

⁵Consider the helicity modulus for the Wilson action $h(\beta) = \frac{\beta}{V} \langle \sum \cos \theta_P \rangle - \frac{\beta^2}{V} \langle (\sum \sin \theta_P)^2 \rangle$; one can show [24] that the first term $\beta \langle \cos \theta \rangle = \beta - \frac{1}{4} + \mathcal{O}(\frac{1}{\beta})$, while the second term turns out to be $\mathcal{O}(\frac{1}{\beta})$. A generalization to the extended action is straightforward.

L	ν
8	0.28(2)
10	0.30(1)
12	0.34(3)

Table 2: Fitted exponent ν from Eq. (62), for increasing lattice size L .

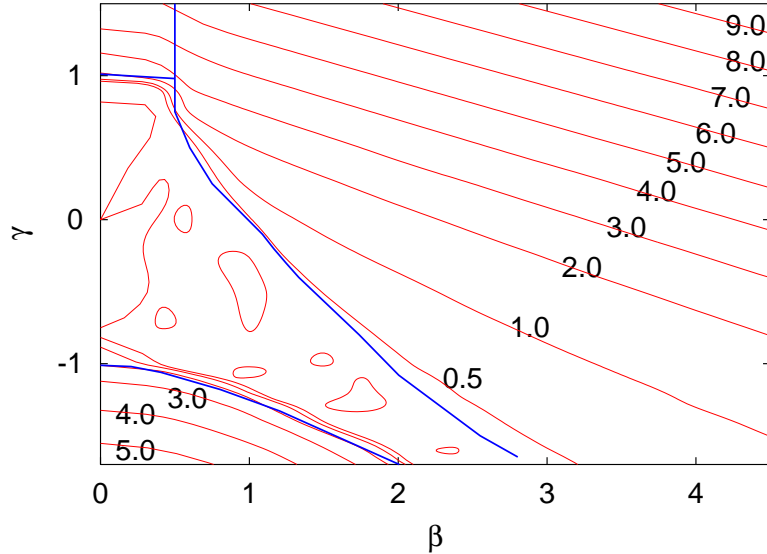


Figure 17: Lines of constant physics (i.e. constant renormalized Coulomb coupling $\beta_R = 1/e_R^2$) in the extended (β, γ) bare coupling plane. The numbers indicate the value of the helicity modulus ($\approx \beta_R$) along the various iso-lines. Solid blue lines indicate the phase boundaries. In the confined phase surrounding the origin, the renormalized β_R is zero.

Going to a more quantitative footing, a first possible test is to compare the values of the renormalized coupling one obtains using different lattice discretizations of the continuum Abelian theory. In [22] a comparison is performed between the Wilson and the Villain action, which shows agreement of $e_R^2(\beta_c^+)$ within errors, thus supporting Cardy's conjecture.

Here we propose a more demanding test: if universality holds, the value of the helicity modulus should be the same along the phase boundary in the extended phase plane. This statement can be motivated by observing that each phase is actually

characterized by some specific infra-red (IR) behavior, and this is all we need to apply the universality hypothesis. Therefore, in order to verify Cardy's conjecture, we studied the *lines of constant physics* in the Coulomb phase of our model, i.e., the lines of equal renormalized coupling. They are shown in Fig. 17.

From this figure we can deduce that Cardy's conjecture is not satisfied. On one hand, in the lower right corner of the phase diagram the lines of constant physics tend to be parallel to the phase boundary, so numerically we should find that the conjecture is roughly verified (in fact a numerical test performed at $\beta = 2.5$ (Fig.11) gives a value of the helicity modulus $h = 0.37(4)$ in agreement with the Wilson axis value Eq. (36)). On the other hand, if we look at values of $\gamma > 0$, it is clear that the helicity modulus grows, thus disproving the conjecture. In order to exhibit this effect, in Fig. 18 we show the helicity modulus as a function of β , for $\gamma = 0.9$: it takes value ~ 2 near the transition, totally incompatible with the Wilson axis value of Section 7.1.

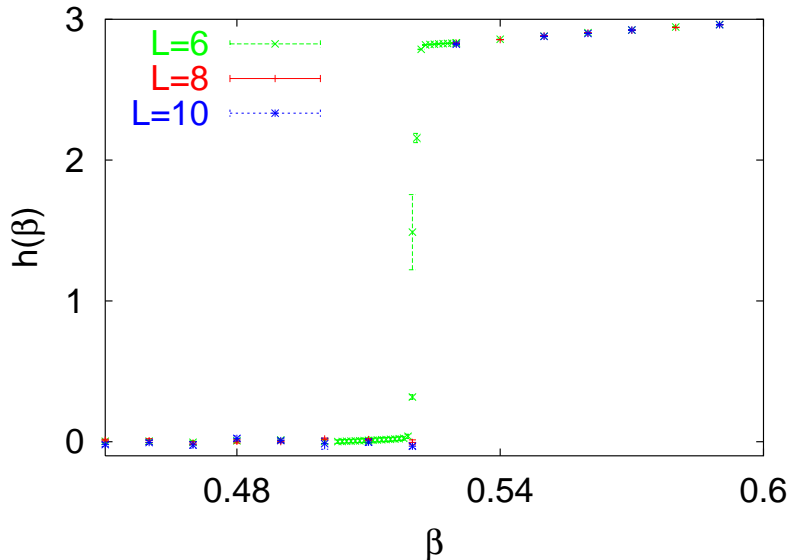


Figure 18: Helicity modulus versus β , at $\gamma = 0.9$ ($6^4, 8^4, 10^4$ lattice).

As a further comment on Fig. 17, it is interesting to observe that the iso-lines, away from the boundaries, are roughly straight with slope $-\frac{1}{4}$ (in Fig. 17 this is realized in the upper right corner): this slope is easily understood considering the helicity modulus $h(\beta, \gamma)$ at weak coupling, where given a value $h(\beta, \gamma) = \tilde{h}$ we find

$$\beta + 4\gamma = \tilde{h} \quad (63)$$

8 Making monopoles with fluxes

Since we have been applying external electromagnetic fluxes to our system, we consider the natural possibility of enforcing the presence of a monopole in the lattice through its flux. Such a possibility is provided by adding an external flux (just like we did in Section 5) but using different boundary conditions, namely *spatial C-periodic b.c.*[26]: when we cross the boundary of the lattice moving in a spatial direction we enter another copy of the lattice whose links are all conjugated

$$U_\mu(x + L_i \hat{e}_i) = U_\mu^*(x), \quad i = 1, 2, 3, \quad \mu = 1, \dots, 4 \quad (64)$$

The conjugation produces the inversion of the orientation of the plaquettes, and also the inversion of the direction of magnetic fluxes. If we try to vary the flux in such a lattice, and we insist on requiring translation invariance, we are faced with a severe restriction: because of the inversion of the flux direction, on the boundaries we need to impose the consistency condition

$$\phi = -\phi \text{ mod } 2\pi \quad (65)$$

so only a flux $\phi = 0$ or $\pi \text{ mod } 2\pi$ can be added. In the latter case the total flux going out of the lattice is 2π , and therefore the presence of one magnetic monopole is enforced in the lattice. What we called ‘flux free energy’ before can now be rephrased as *monopole free energy*, and we set

$$F(\phi = \pi, \beta) - F(\phi = 0, \beta) = L_4 F_{\text{monop.}}(\beta) \quad (66)$$

i.e., $F_{\text{monop.}}$ is the free energy per time-slice, or, in more suggestive terms, the free energy per unit of monopole current.

In Fig. 19 we present the numerical determination of this quantity along the Wilson axis. First of all, observe that it is an order parameter, as expected: the monopole free energy is zero in the confined phase and different from zero in the Coulomb phase. The finite size effects are clearly visible, as for the helicity modulus. In the Coulomb phase, as we derived in the previous section, we have finite size effects proportional to $1/L$ (at leading order). The main qualitative difference w.r.t. the helicity modulus is that these lines intersect each other (at $\beta \sim 1.0125$). We will comment about this during the data analysis.

We now make the same kind of analysis we performed for the helicity modulus: first we assume that the transition is first-order, therefore we fit the data of the monopole free energy in the range $\beta \leq \beta_c$, according to Eq. (31). The results are: $m_+ = 0.08(2)$, $\Delta f'/6 = 0.028(5)$, $\log X = 0.50(8)$, $\beta_c = 1.0115(3)$, $\alpha_1 \simeq 14.7$, $\alpha_2 \simeq (5.7)^4$. In Fig. 20, on the left, we show the result of the fit: the agreement is excellent, and we can also observe the approximately straight behavior (in log-scale) of the order parameter away from β_c , signaling the first-order nature of the transition.

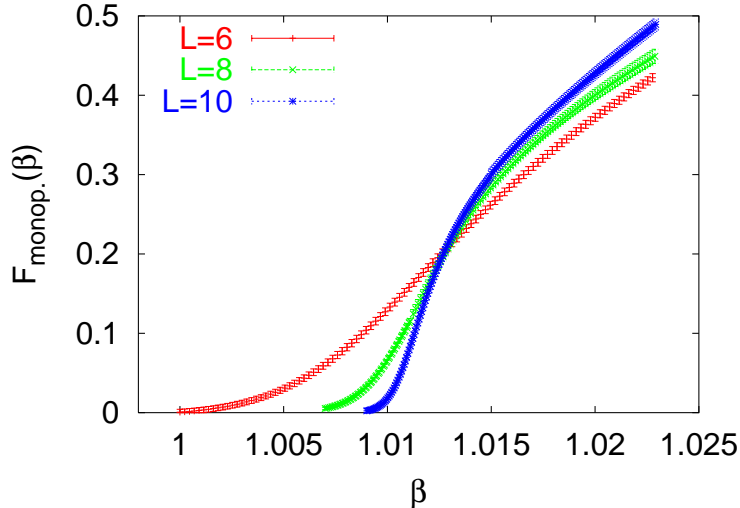


Figure 19: Monopole free energy as a function of β for different lattice sizes ($L = 6, 8, 10$).

Going to the second-order analysis, we observe that the data show good collapse for $\beta < \beta_c$ only (see Fig. 20 on the right) when β is rescaled according to Eq. (45) for a ‘test’ value of $\nu \sim 0.45$. We also observe that the crossing of the curves of an order parameter at the transition is most unusual for a second-order phase transition: the usual behavior is that of a family of non-intersecting curves approaching the thermodynamic limit.

Also in this case, therefore, we observe an indication in favor of the first-order nature of the transition.

As a numerical algorithm, the chain rule (Eq. (23)) was used also in this case. It is interesting to note that all the individual ratios violate the boundary consistency condition Eq. (65) we mentioned at the beginning; only the product of all of them (corresponding to a flux of π) respects it. To obtain the free energy over a range of β values, we simply apply the Ferrenberg-Swendsen reweighting algorithm to each ratio of the chain and then perform the multiplication.

We conclude this section with some notes about other strategies used in the literature to enforce the presence of a monopole in the lattice.

The Pisa group [27] builds a magnetically charged operator μ which satisfies the following equation

$$\mu(\vec{y}, t) |\vec{A}(\vec{x}, t)\rangle = |\vec{A}(\vec{x}, t) + \frac{1}{e}\vec{b}(\vec{x} - \vec{y})\rangle \quad (67)$$

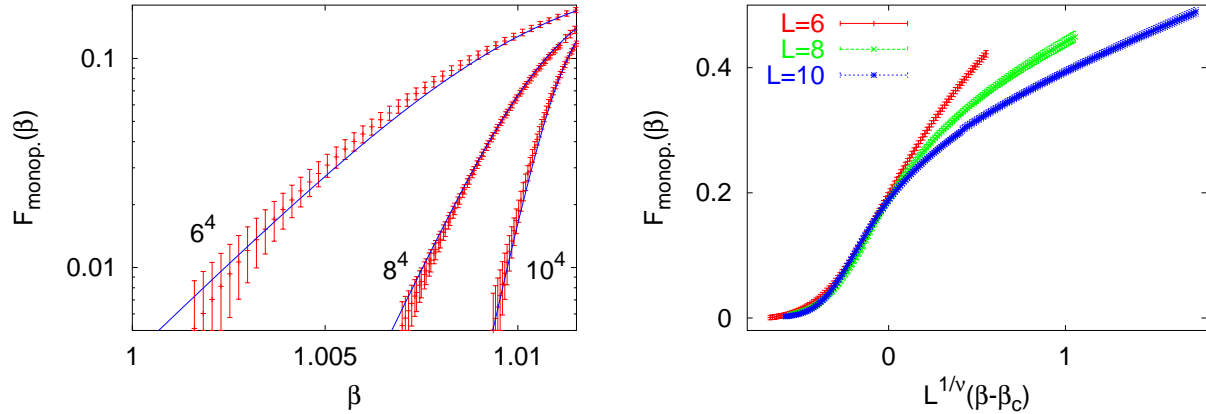


Figure 20: Comparison of the first (left) and second (right) order scenarios for the monopole free energy data.

where $\vec{A}(x)$ is the vector potential and $\vec{b}(\vec{x} - \vec{y})$ is the field of a monopole of charge $\frac{2\pi}{e}$ sitting at \vec{y} ; $\mu(\vec{y}, t)$ can therefore be written as

$$\mu(\vec{y}, t) = e^{\frac{i}{e} \int d^3x \vec{E}(\vec{x}, t) \vec{b}(\vec{x} - \vec{y})} \quad (68)$$

The actual *disorder* parameter is built considering a discretized version of Eq. (68). Then the two-point function

$$D(t) = \langle \mu(\vec{x}, t) \bar{\mu}(\vec{x}, 0) \rangle \quad (69)$$

describes the propagation of a monopole in time from 0 to t . Finally, considering the usual ansatz

$$D(t) = ce^{-Mt} + \langle \mu \rangle^2 \quad (70)$$

one focuses on the measurement of $\langle \mu \rangle$ as a function of β , which should provide the signature for monopole condensation.

The boundary conditions used are pure periodic in the spatial directions and C -periodic in time direction. Given a time-slice, the total flux going out from the boundaries must be zero. This means that when a monopole is added by hand at position \vec{y} , an anti-monopole is also automatically created somewhere. In our case it is possible to enforce the presence of only one monopole in the lattice because of the C -periodic spatial boundary conditions. A second remark attains the property of translation invariance: in our case no input about the location of the monopole in the system is given; this choice is taken dynamically by the system.

In order now to compare quantitatively the two constructions, we show in Fig. 21 the derivative w.r.t. β of the monopole free energy, which is the quantity that

directly compares to the Pisa group data. It is interesting to observe that, for lattices of comparable size, their peak is roughly twice as high than ours, which is compatible with the presence of a pair of monopoles instead of only one. Furthermore, the width of the peak is also much larger, probably as an effect of the discretization of the monopole field.

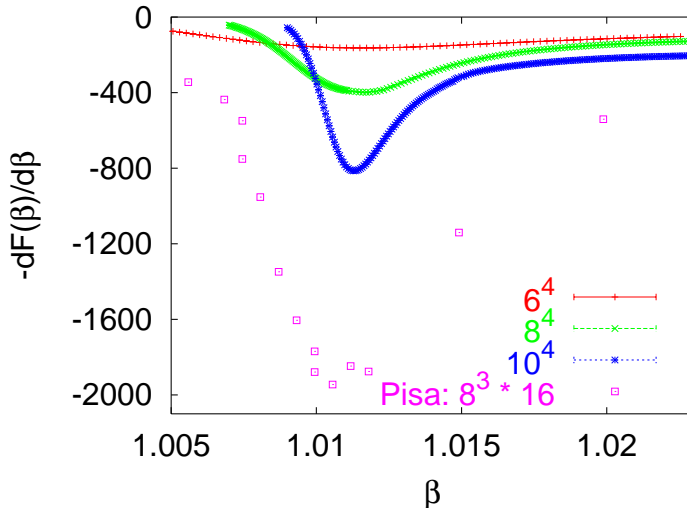


Figure 21: Comparison of our data (the first derivative w.r.t. β of the monopole free energy shown in Fig. 19) with Di Giacomo et al. [27].

We can also compare the value of the monopole free energy in the classical limit. In [28] a computation of the classical monopole free energy in the weak coupling approximation is performed. We numerically computed the same quantity by just cooling the system (limit $\beta \rightarrow \infty$, obtained by minimizing iteratively the action while visiting the links) and measuring the classical monopole *free energy per time-slice* $S_{\text{cl.}}/L_4$: this is the relevant quantity we compare. Our results are shown in Fig. 22 for the Wilson action. We obtain

$$S_{\text{cl.}}/L_4 = 4.695 - \frac{1.20}{L} \quad (71)$$

Ref.[27], Eq. (58), provides an expression corresponding to our $(-S_{\text{cl.}})$ in the weak coupling approximation. Since the lattice there is of size $L^3 \cdot 2L$, we consider

$$S_{\text{cl.}}/L_4 = \frac{-(-5.05L + 4.771)}{L_4} = 2.525 - \frac{2.386}{L} \quad (72)$$

The rather large difference in the constant terms between Eq. (72) and Eq. (71) should come as no surprise. We assign it to the discretization of the monopole field

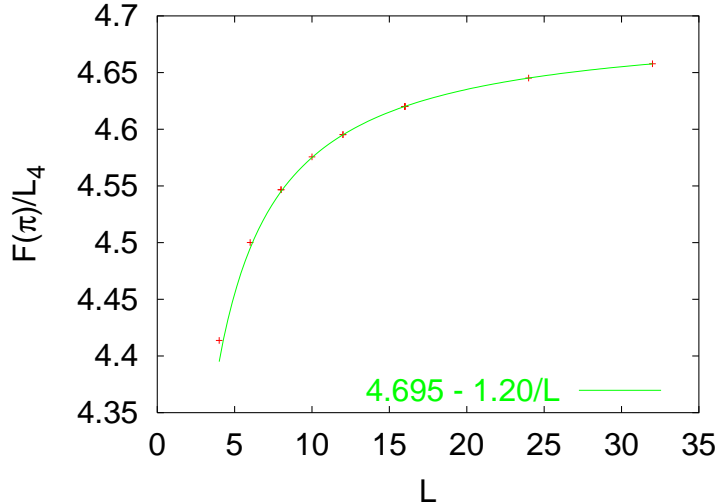


Figure 22: Lattice measurement of the classical monopole free energy.

used in the Pisa group computation: since the monopole energy is UV-divergent, small changes in the monopole field at short distance will have a large impact. Interestingly, the $1/L$ terms, which are insensitive to the monopole field discretization, are very nearly in the ratio 1:2, again in agreement with our interpretation of the two constructions.

Jersak et. al. [25] perform an *exact duality transformation* of the Villain action, imposing spatial C -periodic boundary conditions in the spatial direction and pure periodic in the time direction. Thus their system is physically identical to ours. They compute the two-point monopole correlation functions in the time direction $D(t)$ and use the ansatz

$$D(t) = ce^{-Mt} + \langle \mu \rangle^2 \quad (73)$$

to extract the monopole mass M and monopole condensate $\langle \mu \rangle$. They measure the monopole condensate as a function of β in the confined region and the monopole mass (again vs. β) in the Coulomb phase. Assuming a second order scenario for the phase transition, a scaling behavior is observed for both quantities as they approach the (conjectured) critical point. First of all, it is interesting to observe that in Fig. 20 (on the right) we find a ‘test’ critical exponent $\nu = 0.45$ which compares very well with the value they find $\nu = 0.49(4)$ for the critical behavior of the monopole mass in the Coulomb phase (Eq. (1.2) in [25]). Moreover, from Fig. 20 (on the left) we deduce a value of the monopole free energy at the transition of about 0.1, which is smaller than the smallest value ~ 0.3 computed in [25] just above the ‘critical’

point. So Ref. [25] was not in a position to see the jump of the monopole mass.

9 Conclusions and perspectives

In this paper, we have followed 't Hooft's viewpoint that twist (or flux) free energies can serve as order parameters for confinement. Twisted boundary conditions were introduced for non-Abelian $SU(N)$ gauge theories. There, the amount of twist is quantized according to the center group Z_N . Here, we have considered the Abelian $U(1)$ theory, and the twist can be continuously varied. Twisted b.c. are equivalent to periodic b.c. plus an external electromagnetic flux; we measure the free energy of such a flux and show that it is an order parameter, which vanishes in the confined phase just like in the Yang-Mills case [29, 17, 30].

Studying the $U(1)$ theory from the perspective of fluxes allows us to make practical and conceptual progress.

On the practical side, we have introduced the helicity modulus for a gauge theory, which represents the response of the system to an infinitesimal external flux. This observable is an order parameter just like the flux free energy. It is simple to measure, and gives a clear signal for the phase transition even on a small lattice, because it makes use of the full extent of the lattice. Moreover, it is simply related to the renormalized coupling. Using this observable, we show that the transition is first-order, with parameters (β_c , latent heat, phase asymmetry) in full agreement with the recent results of [21, 11]. Note that a jump in a non-local order parameter is not, by itself, the signature of a first-order transition. For example, the helicity modulus of the XY model has a (universal) jump at T_c , although the transition is continuous. The first-order signature comes from the exponential (not power-law) behavior of the finite-size effects, as seen in Fig. 14, left.

From the helicity modulus we extract the renormalized charge $e_R^2 = 2.305(15)$ at the transition point with high precision. We map lines of constant renormalized charge in the (β, γ) coupling plane, and disprove the conjecture by Cardy [2] of the universality of e_R along the transition line.

On the conceptual side, we have shown that a consistent description of the $U(1)$ phase transition can be given without referring to magnetic monopoles, using the notion of flux only. In fact, we can build a monopole from flux, and force a monopole into the system by adjusting the boundary conditions to produce a 2π outgoing flux, preserving gauge and translation invariance. We compare this elegant approach with earlier constructions.

The vanishing of the monopole free energy in the confined phase is thus accom-

panied by the vanishing of the flux free energy. Flux sectors, characteristic of the Coulomb phase, disappear. The condensation of monopoles is accompanied by the condensation of vortices or Dirac sheets.

From our study, it is clear that monopoles are not the only choice of topological defect to describe the phase transition. Fluxes and monopoles are to each other like “chicken and egg”, and assigning preeminence to one or the other is a subjective matter in the $U(1)$ case. In the Yang-Mills case, fluxes are more commonly called center vortices, and monopoles become Abelian monopoles after Abelian gauge-fixing and projection. Again they are similarly related to each other. This time, the center vortices may be given some preference, because their free energy is a gauge-invariant, UV-regular order parameter [17, 30].

Several extensions of our work come to mind. The dimension of the system could be reduced to 3. The helicity modulus is still an order parameter, but at zero temperature it is always zero, since the theory is always confining [31]. At finite temperature however, a deconfinement transition occurs [32]. This transition is difficult to study numerically, because according to the Svetitsky-Yaffe conjecture [33] it belongs to the Kosterlitz-Thouless universality class and is of infinite order. The $U(1)$ helicity modulus, which in this case directly maps onto the XY helicity modulus, would be a very appropriate order parameter. Another direction would be to measure the helicity modulus in a Yang-Mills theory after Abelian projection. It may give information about the deconfinement transition as the temperature is varied [34].

Finally, the picture in terms of fluxes is the natural environment to introduce a $U(1)$ *topological charge*. Let $\Phi_{\mu\nu}$ be the flux through the orientations μ, ν , and define $\Phi_{0i} = k_i$, and $\epsilon_{ijk}\Phi_{jk} = m_i$. The topological charge Q can be expressed as

$$Q = k \cdot m \tag{74}$$

Even though instantons do not exist in the $U(1)$ theory on R^4 , the topological charge above, defined as the integrated second Chern character, can be non-zero on a torus in the presence of fluxes.⁶ This would provide a natural laboratory to study the topological charge susceptibility or θ -vacua [35], at least in the Coulomb phase.

10 ACKNOWLEDGEMENTS

We gratefully acknowledge Jürg Fröhlich and Oliver Jahn for useful comments and discussions.

⁶We thank O. Jahn and P. van Baal for clarifying this point.

References

- [1] J. V. Jose, L. P. Kadanoff, S. Kirkpatrick and D. R. Nelson, Phys. Rev. B **16**, 1217 (1977).
- [2] J. L. Cardy, Nucl. Phys. B **170**, 369 (1980).
- [3] J. Froehlich and T. Spencer, in ‘Scaling and Self-Similarity in Physics’, J. Froehlich (ed.), Progr. in Phys., Birkhauser 1983, pg.29
- [4] T. A. DeGrand and D. Toussaint, Phys. Rev. D **22**, 2478 (1980).
- [5] T. Banks, R. Myerson and J. B. Kogut, Nucl. Phys. B **129**, 493 (1977).
- [6] G. ’t Hooft, Nucl. Phys. B **153**, 141 (1979).
- [7] D. R. Nelson and J. M. Kosterlitz, Phys. Rev. Lett. **39**, 1201 (1977).
- [8] P. de Forcrand and M. Vettorazzo, Nucl. Phys. Proc. Suppl. **119** (2003) 715 [arXiv:hep-lat/0209087].
- [9] G. Bhanot, Phys. Rev. D **24**, 461 (1981).
- [10] I. Campos, A. Cruz and A. Tarancon, Nucl. Phys. B **528**, 325 (1998) [arXiv:hep-lat/9803007].
- [11] G. Arnold, B. Bunk, T. Lippert and K. Schilling, Nucl. Phys. Proc. Suppl. **119**, 864 (2003) [arXiv:hep-lat/0210010].
- [12] H. G. Evertz, J. Jersak, T. Neuhaus and P. M. Zerwas, Nucl. Phys. B **251**, 279 (1985).
- [13] R. Sinclair, Phys. Rev. D **45** (1992) 2098.
- [14] B. A. Berg and T. Neuhaus, Phys. Lett. B **267**, 249 (1991).
- [15] U. M. Heller, Nucl. Phys. Proc. Suppl. **4** (1988) 417.
- [16] P. Cea and L. Cosmai, Phys. Rev. D **43** (1991) 620.
- [17] P. de Forcrand, M. D’Elia and M. Pepe, Phys. Rev. Lett. **86**, 1438 (2001) [arXiv:hep-lat/0007034].
- [18] A. M. Ferrenberg and R. H. Swendsen, Phys. Rev. Lett. **61** (1988) 2635.
- [19] C. Borgs and R. Kotecky, J. Stat. Phys. **61**, 79 (1990).

- [20] C. Borgs and R. Kotecky, Phys. Rev. Lett. **68**, 1734 (1992).
- [21] G. Arnold, T. Lippert, K. Schilling and T. Neuhaus, Nucl. Phys. Proc. Suppl. **94**, 651 (2001) [arXiv:hep-lat/0011058].
- [22] G. Cella, U. M. Heller, V. K. Mitrjushkin and A. Vicere, Phys. Rev. D **56**, 3896 (1997) [arXiv:hep-lat/9704012].
- [23] J. Cox, W. Franzki, J. Jersak, C. B. Lang, T. Neuhaus and P. W. Stephenson, Nucl. Phys. B **499**, 371 (1997) [arXiv:hep-lat/9701005].
- [24] R. Horsley and U. Wolff, Phys. Lett. B **105**, 290 (1981).
- [25] J. Jersak, T. Neuhaus and H. Pfeiffer, Phys. Rev. D **60**, 054502 (1999) [arXiv:hep-lat/9903034].
- [26] A. C. Davis, T. W. Kibble, A. Rajantie and H. Shanahan, JHEP **0011**, 010 (2000) [arXiv:hep-lat/0009037].
- [27] A. Di Giacomo and G. Paffuti, Phys. Rev. D **56** (1997) 6816 [arXiv:hep-lat/9707003].
- [28] L. Del Debbio, A. Di Giacomo and G. Paffuti, Phys. Lett. B **349** (1995) 513 [arXiv:hep-lat/9403013].
- [29] T. G. Kovacs and E. T. Tomboulis, Phys. Rev. Lett. **85** (2000) 704 [arXiv:hep-lat/0002004].
- [30] P. De Forcrand and L. Von Smekal, Nucl. Phys. Proc. Suppl. **106** (2002) 619 [arXiv:hep-lat/0110135].
- [31] A. M. Polyakov, Nucl. Phys. B **120**, 429 (1977).
- [32] N. Parga, Phys. Lett. B **107** (1981) 442; M. N. Chernodub, E. M. Ilgenfritz and A. Schiller, Phys. Rev. D **64** (2001) 054507 [arXiv:hep-lat/0105021].
- [33] B. Svetitsky and L. G. Yaffe, Nucl. Phys. B **210** (1982) 423.
- [34] M. Vettorazzo and Ph. de Forcrand, proceedings of the Lattice 03 conference (Tsukuba, June 2003) [arXiv:hep-lat/0311007].
- [35] G. 't Hooft, Nucl. Phys. B **190** (1981) 455.

APPENDIX: Summary of the simulations performed

L	β	meas.	update	observable
4	(1.2, 0)	10^5	multi-canonical	flux distribution
4	(0.8, 0)	10^5	multi-canonical	flux distribution
4	(0.8, 0)	10^4	snake update	flux free energy
4	(1.1, 0)	10^4	snake update	flux free energy
4	(1.5, 0)	10^4	snake update	flux free energy
4	(1.0, -1.5)	10^4	snake update	flux free energy
6	(0.99 \div 1.03, 0)	10^5	1 h.b., 4 o.r.	helicity modulus
6	(0.99 \div 1.03, 0)	10^5	snake update	monopole free energy
6	(1.03 \div 1.30, 0)	10^5	1 h.b., 4 o.r.	helicity modulus
6	(2.5, -0.9 \div -2.4)	10^5	1 h.b., 4 o.r.	helicity modulus
8	(1.0 \div 1.03, 0)	10^5	1 h.b., 4 o.r.	helicity modulus
8	(1.0 \div 1.03, 0)	10^5	snake update	monopole free energy
8	(2.5, -0.9 \div -2.4)	10^5	1 h.b., 4 o.r.	helicity modulus
10	(1.005 \div 1.03, 0)	10^5	1 h.b., 4 o.r.	helicity modulus
10	(1.005 \div 1.03, 0)	10^5	snake update	monopole free energy
10	(1.03 \div 1.30, 0)	10^5	1 h.b., 4 o.r.	helicity modulus
10	(2.5, -0.9 \div -2.4)	10^5	1 h.b., 4 o.r.	helicity modulus
12	(1.008 \div 1.03, 0)	10^5	1 h.b., 4 o.r.	helicity modulus
12	(2.5, -0.9 \div -2.4)	10^5	1 h.b., 4 o.r.	helicity modulus
32	(1.0111331, 0)	10^5	1 h.b., 4 o.r.	helicity modulus

Table 3: Summary of the numerical simulations performed for this paper. The four columns contain respectively the lattice size L , the Wilson and extended couplings (β, γ) (when two values of β or γ are indicated, e.g. (0.99 \div 1.02, 0), a grid of points is meant in between), the number of measurements, the updating algorithm (‘h.b.’ indicates heat-bath, ‘o.r.’ over-relaxation; for the ‘snake update’ [17], see Sec.5), the main observable.